Determining a Robust Lower Bound on Voltage Magnitudes to Enhance Voltage Stability

Katharina Kaiser*†, Johanna Vorwerk*, Marc Hohmann‡, Stavros Karagiannopoulos‡, Fabian Streiff‡, Gabriela Hug*
*EEH - Power Systems Laboratory, ETH Zurich, Physikstrasse 3, 8092 Zurich, Switzerland
‡Swissgrid AG, Bleichemattstrasse 31, 5001 Aarau, Switzerland
†katharina.kaiser@eeh.ee.ethz.ch

***Abstract*—The bounds safeguarding the steady-state voltage stability of a power system must resist a wide variety of operating conditions. While the upper voltage magnitude bound is given by hardware restrictions, the lower bound must ensure that the loadability limit of the system is not exceeded. Capturing this limit for different load and generation patterns in a single voltage magnitude value is complex. In this work, the operating point which leads to the optimal lower voltage bound is first determined, and an iterative method for identifying this operating point is proposed. The method traces the transfer limit surface, which separates the feasible from the infeasible region of the parameter space, such that the minimum voltage magnitude at the maximum loading point increases. Both saddle-node bifurcations and limits caused by generators reaching their reactive power limits are taken into account. The method is validated on an IEEE 9-bus test case and then applied to the actual Swiss transmission grid with more than 300 buses.**

***Index Terms*—Voltage stability, saddle-node bifurcation, switching loadability limit**

I. Introduction

The growing penetration of renewable energy sources and the electrification of the transportation and heating sectors are challenging the stable operation of power systems [1]. Voltage instability is one of the mechanisms that can cause large-scale blackouts, as occurred in Greece in 2004 [2]. A common approach to mitigate the risk of a blackout is ensuring that all bus voltage magnitudes are higher than a predetermined lower threshold, both in offline studies and during real-time operation. As the voltages at the loadability limit differ depending on the loading condition, the current thresholds must be reevaluated to account for the changing load, generation, and transit patterns. Usually, the threshold is specified by analyzing a limited number of loading directions, i.e., load distributions, in a brute force fashion, using, e.g., the continuation power flow or direct methods [3]. However, the selected directions might not represent the worst-case scenario, and the resulting bound potentially fails to ensure stable operation. Therefore, an alternative method for determining a robust and reliable bound is desirable.

Besides a single lower voltage bound, voltage stability indices provide another solution to track stability. They aim to capture the system's distance to instability at a particular operating point in a single value [3]. A standard index is the loading margin, which describes the distance to the maximum loading point of a specified load increase direction. Other examples are the eigenvalues or the minimum singular value (MSV) of the power flow Jacobian [3]. The authors of [4] and [5] demonstrate the usefulness of the MSV by constraining it in an optimal power flow formulation. However, determining the correct bound of such indices is difficult. In particular, considering reactive power generation limits complicates determining a threshold for eigenvalues and MSVs. In addition, complex indices are less intuitive to interpret by system operators than voltage magnitudes.

Instead of analyzing how close a particular operating point is to instability, the authors of [6] suggest defining a voltage security region, i.e., viable power injections, for which specified voltage magnitude bounds are met. However, this does not resolve how the lower bound should be defined.

In this work, we aim to find a lower voltage bound by developing an algorithm that traces the transfer limit surface. This is a hypersurface in the active and reactive power injection space, consisting of the maximum loading points of all possible loading directions [7]. The contributions of our work are threefold:

- First, we define the operating point that determines the optimal lower bound for the voltage magnitudes.
- Then, we suggest an iterative algorithm to find this operating point. The algorithm considers the reactive power limits of generators, is based on the AC power flow model and is implementable using standard tools.
- Finally, we apply and test the proposed method on the IEEE 9-bus test case and the Swiss transmission grid.

The remainder of the paper is structured as follows: In Section II, we discuss the operating condition that results in a robust lower voltage bound. Section III presents the developed algorithm and its mathematical formulation. Section IV gives the results of the performed case studies and Section V concludes the work.

II. Most Critical Operating Point

Finding a lower voltage magnitude bound that guarantees global voltage stability is a challenging task. The loadability limit of a power system is not one operating point, but rather a set of different critical loading conditions that are close to instability. For each of these points, the bus voltage magnitudes differ. In this section, we discuss which operating condition needs to be found to define a robust bound.

The 9-bus system in Fig. 1 serves as an illustrative example to study and determine the most critical operating point. Fig. 2 visualizes the P-V analyses of five different loading directions. A loading direction describes the mapping of the total load p_L^{tot} to the power at each bus. Table I specifies the distribution of the total load in the given example. The

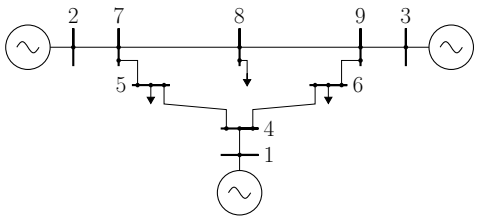

Fig. 1. IEEE 9-bus test system [9].

value $d_{L,i}$ denotes the share of load power consumed at bus i. Different load power factors, expressed in terms of different values for $\tan\phi$, increase the variety in the voltage magnitudes at the maximum loading point. The generators at buses 1 to 3 contribute 70 %, 20 %, and 10 % of the total load power, respectively, and the slack bus balances active power losses. The reactive power of the generators is unlimited.

To study different loadability limits, the following procedure is executed: For each loading direction, the system's load power is incremented starting from no-load condition, while the load and generation shares are kept constant. The power flow problem is repeatedly solved using the Newton-Raphson method (NR). The evaluation stops when the NR cannot find a voltage regular solution for further load power increases. A solution is voltage regular if the V-Q sensitivities for all buses are greater than or equal to zero [8]. Specifically, if reactive power is injected at bus i, it must hold that $\Delta V_i/\Delta Q_i > 0$ and $\Delta V_j/\Delta Q_i \geq 0$ for all buses $j \neq i$.

For the following considerations, several representations are obtained: Fig. 2 depicts the evaluated points for each loading direction, denoted by their respective numbers. Fig. 3a shows the P-V curves, also known as nose curves, for the load buses. Each plot corresponds to one loading direction and depicts the voltage magnitudes of the load buses over the total load power at the evaluated points. Fig. 3b summarizes the voltage magnitudes for each load bus at the maximum loading points, i.e., the operating point at the right end of each P-V curve (note the color coding).

Based on the last illustration, the optimal lower voltage bound is determined by the maximum loading point for which the minimum voltage magnitude is highest. In our example, this corresponds to scenario 5. Choosing the minimum bus voltage magnitude at this operating point as the lower voltage bound ensures that the system will not reach its loadability limit for all other loading directions. Note that a safety margin should be added to also guarantee stability for loading direction 5. If a voltage bound lower than the dashed red line in Fig. 3b was chosen, the system could exceed its loadability limit for loading direction 5 without detecting it.

This example considers only five loading directions. For a robust lower voltage bound, all loadability limits, i.e., all points on the transfer limit surface, must be considered. Generalizing the above findings, the most critical operating condition is the point in the P-Q space that is on the verge of stability and for which the minimum out of all bus voltage magnitudes is highest.

III. Proposed Methodology

This section proposes a method to find the previously defined critical operating point. A condition ensuring that

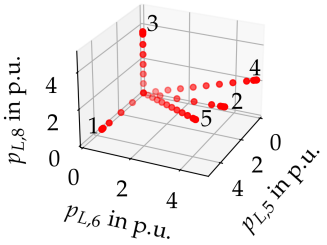

Fig. 2. Visualization of the loading directions in the load active power space.

TABLE I
Specifications for each loading direction

#	$d_{L,5}$	$d_{L,6}$	$d_{L,8}$	$\tan\phi$
1	1	0	0	0.6
2	0.1	0.8	0.1	0.4
3	0.2	0.1	0.7	0.4
4	0.1	0.6	0.3	-0.2
5	0.4	0.4	0.2	-0.2

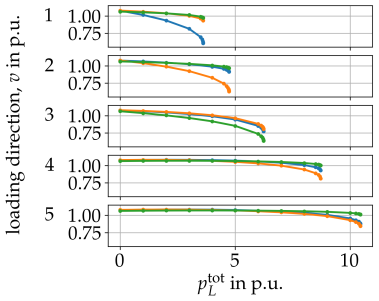

(a) P-V curves for the load buses.

(b) Summary of the maximum loading points.

Fig. 3. Results of the P-V analyses.

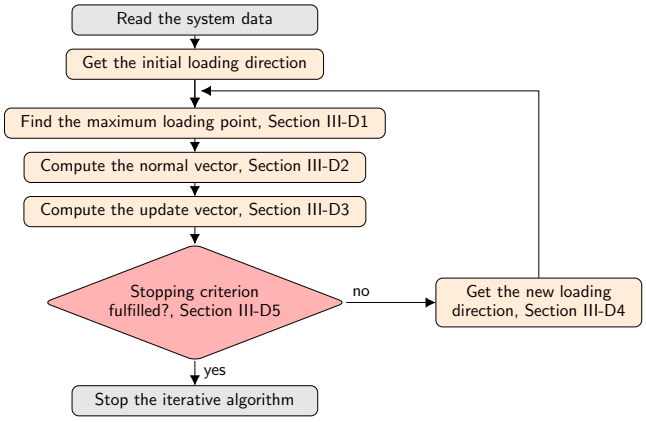

Fig. 4. Flowchart of the proposed iterative algorithm.

an operating point is on the transfer limit surface cannot be easily included in an optimization problem, particularly when considering reactive power generation limits. Therefore, the proposed algorithm traces the hypersurface by iteratively evaluating different loading directions. The update vector, which determines the next loading direction, is chosen such that the minimum voltage magnitude at the loadability limit increases. Before discussing the assumptions, the model, and the steps in detail, an illustrative example demonstrates the algorithm that is also summarized in Fig. 4.

A. Illustrative Example

Fig. 5 demonstrates the iterative scheme for a 2-bus system consisting of a slack bus with voltage 1 p.u., a lossless line with reactance 0.25 p.u., and a load described by the active power p_L and reactive power q_L.

The upper subplots show three iterations performed in the load power space. The green shaded area represents the feasible space that is bounded by the gray parabola consisting

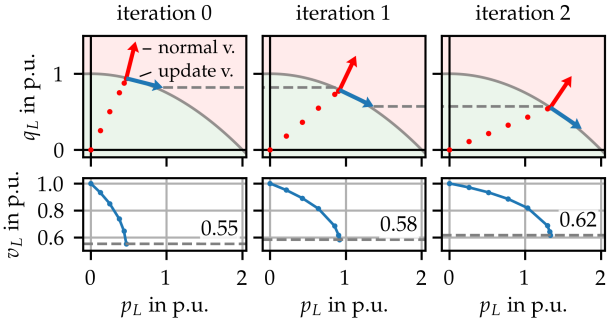

Fig. 5. Iterative scheme for a 2-bus system. Top: Solution space for three iterations from left to right. Bottom: Corresponding P-V curves. The voltage magnitude at the loadability limit for each iteration is stated in each subplot.

of the maximum loading points for varying load power factors. The initial loading direction is chosen arbitrarily. The maximum loading point, i.e., the point lying on the boundary, is determined using repeated power flow calculations, represented by the red points. Having reached the boundary, the next step is to compute an update vector $\begin{bmatrix}\Delta p_L & \Delta q_L\end{bmatrix}^\intercal$ that points to the maximum loading point of the next iteration and should therefore be tangent to the loadability boundary. Thus, the normal vector to the parabola is computed (red arrow), and the update vector is constrained to be orthogonal to this normal vector. Based on the linearized power flow equations, which describe the impact of a change in power injections on the voltage magnitudes, the algorithm chooses the update vector such that it leads to an increase in voltage magnitude at the load bus. A pre-defined step size is applied to the update vector and the next loading direction is found.

The subplots on the bottom of Fig. 5 show the corresponding P-V curve for the load bus in each iteration. The bus voltage magnitude v_L at the maximum loading point increases from 0.55 p.u. to 0.62 p.u., which is the desired behavior of the algorithm.

B. Assumptions

The formulation of the proposed algorithm is built on several assumptions: (i) The three-phase system is balanced and in a steady state at each operating point. (ii) There is either one generator, one load, or no device connected to each bus. (iii) Loads only consume active and reactive power. Preliminary studies showed that the algorithm chooses the least inductive behavior from a predefined range of power factors. Thus, the load power factors are fixed to the least inductive value in the predefined range. Generators inject active power, but they might inject or consume reactive power. (iv) Additionally, the generator voltage setpoints are constant. (v) Only power limits on loads and generators are considered. Other types, such as line flow constraints, are neglected. (vi) Finally, the grid topology is fixed and the results are only valid for that particular grid topology.

C. Power Flow Model

Since the proposed algorithm is based on iterative solutions of the power flow problem, we here give the mathematical formulation that is solved at each iteration. Matrices are denoted by bold capital letters $\mathbf{X}$, while vectors are lowercase symbols $\mathbf{x}$. The system state vector $\mathbf{x} = \begin{bmatrix}\boldsymbol{\theta} & \mathbf{v}\end{bmatrix}^\intercal$ includes the voltage angles and magnitudes for each bus. The reduced vector $\mathbf{x_u}$ only contains the variables for the unknown voltage angles and magnitudes, i.e., the voltage angle and magnitude for the slack bus and the voltage magnitudes for generator buses under voltage control are omitted. The functions for the active and reactive power flow out of each bus are summarized in $\mathbf{g}(\mathbf{x}) = \begin{bmatrix}\mathbf{p}(\mathbf{x}) & \mathbf{q}(\mathbf{x})\end{bmatrix}^\intercal$, with:

$$p_i(\mathbf{x}) = v_i \sum_{j\in\mathcal{I}} v_j(G_{ij}\cos\theta_{ij} + B_{ij}\sin\theta_{ij}), \tag{1a}$$

$$q_i(\mathbf{x}) = v_i \sum_{j\in\mathcal{I}} v_j(G_{ij}\sin\theta_{ij} - B_{ij}\cos\theta_{ij}), \tag{1b}$$

for each bus i. $\mathcal{I}$ is the set of buses bus i connects to, including bus i itself. Variables v_i and v_j are the voltage magnitudes at buses i and j, and $\theta_{ij} = \theta_i - \theta_j$ denotes the voltage angle difference between the corresponding buses. The values for G_{ij} and B_{ij} are determined by the admittance matrix $\mathbf{Y} = \mathbf{G} + j\mathbf{B}$. Substituting the known voltage values, the power balance equations simplify to $\mathbf{g_s}(\mathbf{x_u}) - \boldsymbol{\rho} = \mathbf{0}$, where the vector $\mathbf{g_s}(\mathbf{x})$ summarizes (1) for buses with a specified power injection, while the parameter vector $\boldsymbol{\rho} = \begin{bmatrix}\mathbf{p_s} & \mathbf{q_s}\end{bmatrix}^\intercal$ summarizes the specified active and reactive power injections.

TABLE II
SETS USED IN THE FORMULATION OF THE ALGORITHM

Set	Description
$\mathcal{N}$	Set of all buses.
$\mathcal{S}$	Slack bus.
$\mathcal{PV}$	Set of buses with generation, excluding the slack bus.
$\mathcal{PQ}_{wL}$	Set of buses without generation and without a connected load.
$\mathcal{PQ}_L$	Set of buses without generation but with a connected load.

D. Iterative Method

1) Determining the Maximum Loading Point: The aim of the first step in the iterative cycle is to find the operating point on the transfer limit surface for a chosen loading direction. Possible methods include repeated power flow calculations, the continuation power flow method, or direct methods [3]. This work uses repeated power flow calculations, even though it might only find an operating point close to but not on the transfer limit surface because NR does not converge when the power flow Jacobian is close to being singular.

In each iteration k, the total load power p_L^{tot} is incremented starting with an initial value of zero. The active and reactive power of the individual loads and generators are set to:

$$p_{L,i} = \min\left(d_{L,i}^k\, p_L^{\text{tot}},\, p_{L,i}^{\max}\right) \qquad \forall\, i \in \mathcal{PQ}_L, \tag{2a}$$

$$q_{L,i} = p_{L,i}\tan\phi_i \qquad \forall\, i \in \mathcal{PQ}_L, \tag{2b}$$

$$p_{G,i} = \min\left[s\, d_{G,i}^k \left(\textstyle\sum_{j\,\in\,\mathcal{PQ}_L} p_{L,j} + \delta\right),\, p_{G,i}^{\max}\right] \qquad \forall\, i \in \mathcal{S}\cup\mathcal{PV}, \tag{2c}$$

for which the different bus types are described in Table II. The variables $d_{L,i}^k$ and $d_{G,i}^k$ represent the share of load and generation at bus i, respectively. They specify the analyzed loading direction in iteration k. Parameters $p_{L,i}^{\max}$ and $p_{G,i}^{\max}$ are the active power limits. If a generator fails to supply its share, the remaining power is distributed among the other generators, accounted for by δ in the formulation. The scaling factor $s \geq 1$

represents a distributed slack to account for losses. If only the slack bus balanced the active power losses, the resulting $d_{G,i}$ would deviate from the desired value.

Once the NR method finds a solution for p_L^{tot}, the inverse of the reduced Jacobian matrix $\mathbf{J_r}$ is computed to check whether the solution is voltage regular. The reduced Jacobian is based on the power flow Jacobian $\mathbf{J}$, which includes the partial derivatives of $\mathbf{g_s(x)}$ with respect to the unknown states $\mathbf{x_u}$. It is determined as follows [10]:

$$\mathbf{J} = \begin{bmatrix} \dfrac{\partial \mathbf{p_s(x)}}{\partial \boldsymbol{\theta}_\mathbf{u}} & \dfrac{\partial \mathbf{p_s(x)}}{\partial \mathbf{v_u}} \\ \dfrac{\partial \mathbf{q_s(x)}}{\partial \boldsymbol{\theta}_\mathbf{u}} & \dfrac{\partial \mathbf{q_s(x)}}{\partial \mathbf{v_u}} \end{bmatrix} = \begin{bmatrix} \mathbf{J_{p\theta}} & \mathbf{J_{pv}} \\ \mathbf{J_{q\theta}} & \mathbf{J_{qv}} \end{bmatrix}, \tag{3}$$

$$\mathbf{J_r} = \mathbf{J_{qv}} - \mathbf{J_{q\theta}}\,\mathbf{J_{p\theta}^{-1}}\,\mathbf{J_{pv}}. \tag{4}$$

The entries of $\mathbf{J_r^{-1}}$ represent the V-Q sensitivities. They have to be greater than or equal to zero for a solution to be considered voltage regular [8]. If no voltage regular solution is found for a specified p_L^{tot}, the increment is reduced until it reaches a lower threshold. Note that generator buses at the reactive power limit, for which the voltage magnitude deviates from the setpoint, are treated as PQ buses.

2) Determining the Normal Vector: The transfer limit surface is the set of maximum loading points in the parameter space, spanned by the parameter vector $\boldsymbol{\rho}$, and consists of multiple smooth hypersurfaces. Each hypersurface corresponds to either a saddle-node bifurcation (SNB) or a switching loadability limit (SLL), also referred to as limit-induced bifurcation [7]. SNBs occur when a stable and an unstable equilibrium coalesce and there is no solution to the power flow problem for further load increase, as, e.g., at the maximum loading points of the P-V curves in Fig. 3a. In such a case, the power flow Jacobian is singular. An SLL occurs when the system becomes immediately unstable after a generator reached its reactive power limit [3].

The normal vector computation is different for the two limit types. Thus, the states of the generators at the maximum loading point are analyzed to determine the type of limit. The buses in $\mathcal{PV}$ are split into three subsets, as described in Table III. If no generator is at its limit, i.e., $\mathcal{PV}_{PVQ}$ is empty, it is an SNB. Otherwise, it is an SLL. The transfer limit surface remains smooth at an intersection, or seam, between an SNB and a single SLL surface. Only when two generator buses simultaneously reach their reactive power limits, the transfer limit surface is non-smooth [7]. However, the authors of [7] show that the effect is negligible. Therefore, the proposed algorithm does not treat duplicate-switching separately.

As already mentioned, $\mathbf{J}$ is singular at an SNB. The normal vector $\mathbf{w}$ to the SNB surface is then the left eigenvector corresponding to the eigenvalue λ that is zero: $\mathbf{w}\,\mathbf{J} = \lambda\,\mathbf{w} = \mathbf{0}$ [11]. In the proposed procedure using repeated power flow calculations, only points for which $\mathbf{J}$ is close to singularity are found. However, the normal vector can still be approximated using the left eigenvector corresponding to the smallest eigenvalue [12].

At an SLL, $\mathbf{J}$ is non-singular, and the normal vector cannot be computed with the zero eigenvalue. However, another method is applicable: The only unknown state for the bus in $\mathcal{PV}_{PVQ}$ is the voltage angle. At the same time, two power balance equations, i.e., the active and the reactive power balance, exist for the node. Therefore, $\mathbf{J}$ has one more row than columns, and there must exist a non-zero row vector $\mathbf{z}$ that fulfills $\mathbf{z}\,\mathbf{J} = \mathbf{0}$ [13]. The authors of [7] conclude that $\mathbf{z}$ is the normal vector to an SLL surface.

TABLE III
SUBSETS OF $\mathcal{PV}$

Set	Description
$\mathcal{PV}_{PV}$	Buses in $\mathcal{PV}$ that are not at the reactive power limit.
$\mathcal{PV}_{PVQ}$	Buses in $\mathcal{PV}$ that are at the reactive power limit while the voltage magnitude still equals the voltage setpoint. The solution is voltage regular when the bus in $\mathcal{PV}_{PVQ}$ is treated as a PV bus, but there are negative sensitivities when treating it as a PQ bus.
$\mathcal{PV}_{PQ}$	Buses in $\mathcal{PV}$ that are at the reactive power limit and are not part of $\mathcal{PV}_{PVQ}$.

3) Determining the Update Vector: The update vector is chosen such that the increase in voltage magnitude is highest for the bus that exhibits the lowest magnitude in the current iteration. Therefore, the following optimization problem determines the update vector:

$$\max_{\boldsymbol{\Delta p},\boldsymbol{\Delta q},\boldsymbol{\Delta\theta},\boldsymbol{\Delta v}} \Delta v_j, \qquad j = \arg\min_{i\,\in\,\mathcal{N}} v_i, \tag{5a}$$

$$\text{s.t.} \sum_{i\,\in\,\mathcal{PQ}\,\cup\,\mathcal{PV}} \Delta p_{n,i}\,\Delta p_i + \sum_{i\,\in\,\mathcal{PQ}\,\cup\,\mathcal{PV}_{PVQ}\,\cup\,\mathcal{PV}_{PQ}} \Delta q_{n,i}\,\Delta q_i = 0, \tag{5b}$$

$$\Delta p_i = \sum_{j\,\in\,\mathcal{N}} \frac{\partial p_i(\mathbf{x})}{\partial \theta_j}\Delta\theta_j + \sum_{j\,\in\,\mathcal{N}} \frac{\partial p_i(\mathbf{x})}{\partial v_j}\Delta v_j,\ \forall\, i \in \mathcal{N}, \tag{5c}$$

$$\Delta q_i = \sum_{j\,\in\,\mathcal{N}} \frac{\partial q_i(\mathbf{x})}{\partial \theta_j}\Delta\theta_j + \sum_{j\,\in\,\mathcal{N}} \frac{\partial q_i(\mathbf{x})}{\partial v_j}\Delta v_j,\ \forall\, i \in \mathcal{N}, \tag{5d}$$

$$\tan\phi_i\,\Delta p_i = \Delta q_i, \qquad \forall\, i \in \mathcal{PQ}_L, \tag{5e}$$

$$-\pi \le \theta_i + \Delta\theta_i \le \pi, \qquad \forall\, i \in \mathcal{N}, \tag{5f}$$

$$p_{G,i}^{\min} \le p_{G,i} + \Delta p_i \le p_{G,i}^{\max}, \qquad \forall\, i \in \mathcal{S}\cup\mathcal{PV}, \tag{5g}$$

$$q_{G,i}^{\min} \le q_{G,i} + \Delta q_i \le q_{G,i}^{\max}, \qquad \forall\, i \in \mathcal{S}\cup\mathcal{PV}, \tag{5h}$$

$$p_{L,i}^{\min} \le p_{L,i} - \Delta p_i \le p_{L,i}^{\max}, \qquad \forall\, i \in \mathcal{PQ}_L, \tag{5i}$$

$$\sum_{i\,\in\,\mathcal{N}} \left((\Delta p_i)^2 + (\Delta q_i)^2\right) \le (\eta^k)^2. \tag{5j}$$

Constraint (5b) ensures that the update vector is orthogonal to the normal vector $\left[\boldsymbol{\Delta p_n}\ \boldsymbol{\Delta q_n}\right]$, i.e., that the update vector lies in the hyperplane approximating the transfer limit surface. Constraints (5c) and (5d) specify the linearized power flow equations, evaluated for the voltages at the current maximum loading point. Constraint (5e) keeps the load power factors constant. The inequality constraint (5f) bounds the voltage angles to $[-\pi,\ \pi]$, while constraints (5g), (5h), and (5i) keep the active and reactive power injections at the approximated new maximum loading point within the specified bounds. Note that a positive Δp_i denotes an increase in power injection. Thus, with $p_i = p_{G,i} - p_{L,i}$, Δp_i is subtracted for loads. Constraint (5j) bounds the Euclidean norm of the change in active and reactive power to a step size η, specified for iteration k. In this work, the step size decays exponentially to achieve a good trade-off between progress and convergence. Additionally, some optimization variables are fixed to zero, as given in Table IV. The bus types are assumed to remain the

TABLE IV
SETTINGS FOR THE OPTIMIZATION VARIABLES

	$\mathcal{S}$	$\mathcal{PV}_{PV}$	$\mathcal{PV}_{PVQ}$	$\mathcal{PV}_{PQ}$	$\mathcal{PQ}_{wL}$	$\mathcal{PQ}_{L}$
Δp_i	free	free	free	free	0	free
Δq_i	free	free	0	0	0	free
$\Delta \theta_i$	0	free	free	free	free	free
Δv_i	0	0	free	free	free	free

same while optimizing. This is required because the normal vector is based on the current set of constraints.

4) New Loading Direction: The load and generation shares $d_{L,i}^{k+1}$ and $d_{G,i}^{k+1}$ for the next iteration are calculated based on the current maximum loading point and the resulting $\left[\mathbf{\Delta p}\ \mathbf{\Delta q}\right]^\intercal$ from the optimization problem according to:

$$d_{L,i}^{k+1} = \frac{p_{L,i} - \Delta p_i}{\sum_{j \in \mathcal{PQ}_L} (p_{L,j} - \Delta p_j)} \qquad \forall i \in \mathcal{PQ}_L, \tag{6a}$$

$$d_{G,i}^{k+1} = \frac{p_{G,i} + \Delta p_i}{\sum_{j \in \mathcal{S} \cup \mathcal{PV}} (p_{G,j} + \Delta p_j)} \qquad \forall i \in \mathcal{S} \cup \mathcal{PV}. \tag{6b}$$

5) Stopping Criterion: If the minimum voltage magnitude stagnates for a specified number of iterations k^{return}, the algorithm returns to the loading direction, that led to the highest value so far. It reevaluates if it can improve further using a smaller step size. The algorithm stops after reaching the predefined maximum number of iterations $k^{\max}$ or the maximum number of returns n^{return}.

IV. CASE STUDIES

Several case studies are conducted to showcase and analyze the performance of the algorithm. Before it is tested on the Swiss transmission system, studies on an IEEE 9-bus test case are conducted and compared to a brute force approach.

A. Test Case Setup & Implementation

The case studies are based on the 9-bus system in Fig. 1 and a snapshot of the Swiss transmission grid, which is provided by the Swiss transmission system operator Swissgrid. Both systems are considered to be lossless for simplicity. The Swiss system is adjusted according to the assumptions in Section III. Two-winding transformers replace three-winding transformers to avoid negative V-Q sensitivities caused by star point buses. The resulting model has 310 buses, including 54 generation buses and 188 load buses.

Table V provides an overview of the conducted case studies. The share of active power per load is variable for all cases, while the load power factors are fixed, as discussed above. Case study 1 examines a system in which the reactive power capabilities of generators are unlimited, i.e., there are no SLLs. Additionally, the share of active power generation per generator is fixed by adding the constraint $\Delta p_i = d_{G,i} \sum_{j \in \mathcal{S} \cup \mathcal{PV}} \Delta p_j$, $\forall i \in \mathcal{PV}$ to (5). This reduces the number of degrees of freedom and enables a more detailed analysis. The generators' reactive power capabilities are limited starting from the second test case, and the generation shares are variable in the last two studies.

The algorithm is implemented in Python, combined with the power system analysis tool PSS®E. Problem (5) is solved using SciPy. For case study 4, (5j) is eliminated and each Δp_i and Δq_i is bounded independently, such that the problem is linear and computations are faster. The results were obtained on an Intel Core i7-1165G7 CPU with 32 GB of RAM.

TABLE V
PARAMETERS AND RESULTING VOLTAGE BOUND OF THE PERFORMED CASE STUDIES

Case study	1	2	3	4
System	9-bus	9-bus	9-bus	Swiss
Settings of the proposed method				
Load share $d_{L,i}$	variable	variable	variable	variable
$\tan \phi_i, \forall i \in \mathcal{PQ}_L$	1/3	1/3	1/3	1/3
Generation share $d_{G,i}$	fixed	fixed	variable	variable
$Q_{G,i}^{\max}, \forall i \in \mathcal{PV}$	unlimited	limited	limited	limited
η^0 in p.u.	0.5	0.5	0.5	0.1
$\eta^{k^{\max}}$ in p.u.	0.05	0.05	0.05	0.0001
$k^{\max}$	100	100	100	300
k^{return}	20	20	20	20
n^{return}	2	2	2	2
Results - maximum $v_{\min}$ at a maximum loading point in p.u.				
Brute force	0.7108	0.8974	0.9486	–
Proposed method	0.7123	0.8964	0.9522	0.9315

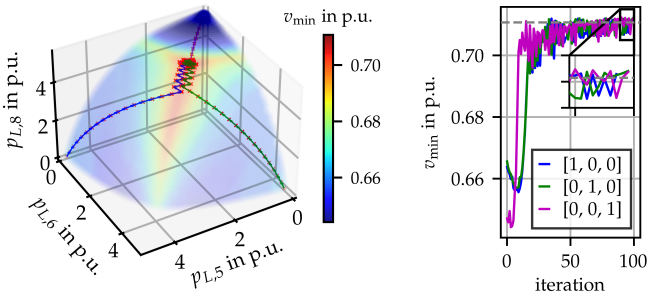

(a) Load active power space. (b) Lowest voltage magnitude.

Fig. 6. Results for case study 1 with unlimited reactive power capabilities and $[d_{G,1}, d_{G,2}, d_{G,3}] = [0.7, 0.2, 0.1]$. The legend in (b) refers to the initial load shares $[d_{L,5}^0, d_{L,6}^0, d_{L,8}^0]$. The dashed line depicts the brute force result.

B. Results

Fig. 6a visualizes the results for case study 1 in the active power space of the load. The surface is derived from a brute force analysis. Its color represents the minimum bus voltage magnitude at the maximum loading point. The proposed algorithm is initialized with three different loading directions, i.e., load shares. The blue, green, and pink arrows represent the update vectors in each iteration. In contrast to Fig. 5, the repeated power flow computations and normal vectors are not depicted. Fig. 6b shows the corresponding minimum voltage magnitudes $v_{\min}$ at the maximum loading points. The oscillations originate from alternations of the bus with the lowest voltage magnitude. The results in Table V indicate comparable voltage bounds for the brute force and the iterative procedure. The corresponding load shares are similar, too (cf. Fig. 6a). While the brute force analysis takes 45 minutes, the iterative algorithm only takes two minutes using the aforementioned computational resources.

In case study 2, the limited reactive power capabilities of generators add SLLs to the transfer limit surface. Fig. 7 presents the results of the simulation. The iterative algorithm converges towards the same loading direction for all three initializations, although the brute force analysis shows higher values for $v_{\min}$ in a different part of the surface. Further

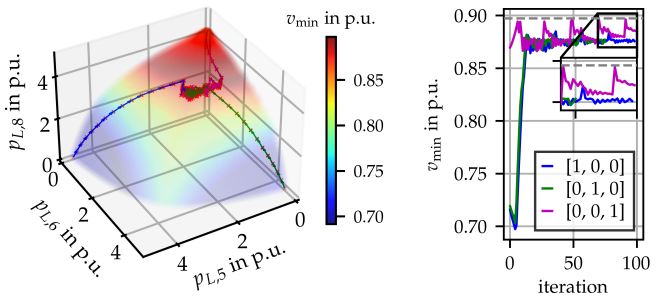

(a) Load active power space. (b) Lowest voltage magnitude.

Fig. 7. Results for case study 2 with limited reactive power capabilities. Settings: $Q_{G,2}^{\max} = Q_{G,3}^{\max} = 100\,\text{Mvar}$ and $[d_{G,1}, d_{G,2}, d_{G,3}] = [0.7, 0.2, 0.1]$.

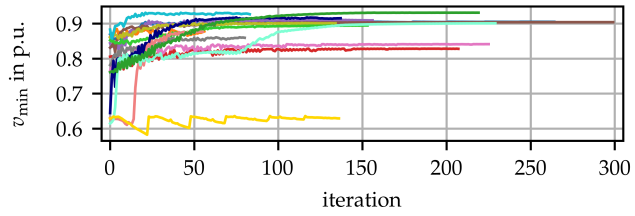

Fig. 8. Results for the Swiss system (case study 4) for 15 different initial loading directions. The colors correspond to different initializations.

investigation reveals that the validity of the linearizations (5c) and (5d) is limited to small power injection changes for some regions, which hinders the algorithm from choosing the correct update vector. Additionally, the importance of the proximity of an SNB maximum loading point to the actual transfer limit surface becomes evident. As the distance to the actual surface reduces, the derived voltage magnitudes decrease, and the accuracy of the normal vector approximation increases. The computation times are comparable to case 1.

Both $d_{L,i}$ and $d_{G,i}$ are variable in case study 3. The algorithm is initialized with ten different randomly chosen loading directions, i.e., load and generation shares. Compared to a brute force analysis of more than $60\,000$ directions with discretized settings for $d_{L,i}$ and $d_{G,i}$, the iterative algorithm finds a loading direction with a higher $v_{\min}$ for eight out of the ten initializations. For the other two initializations, the maximum $v_{\min}$ is $4.4\,\%$ below the brute force result. While the computation time for the brute force method exceeds 6 hours, it ranges from $127\,\text{s}$ to $156\,\text{s}$ for the proposed scheme.

For the final case study 4, a proper brute force analysis is not possible due to the high-dimensional parameter space. 15 randomly chosen initial loading directions are evaluated using the proposed algorithm. Fig. 8 shows the results for $v_{\min}$ at the maximum loading point per iteration. Each curve corresponds to a different initialization. The results demonstrate that the method generally functions for a real grid. However, the performance depends on the initial direction. Drawing meaningful conclusions for the Swiss system requires a more profound selection of the initializations and the settings. For example, the load power factors are essential as a less inductive or capacitive system becomes voltage unstable at higher voltages. In general, if the highest $v_{\min}$ found exceeds the current lower voltage bound, immediate action must be taken to ensure stable operation at all times. On the other hand, if it is lower than the current bound, this indicates that there is potential for higher loading scenarios and a more economical grid operation.

V. Conclusion

Voltage stability is a fundamental requirement for reliably operating a power system. This paper defines the critical operating point for setting a robust lower voltage magnitude bound. It is the operating point on the transfer limit surface for which the minimum out of all bus voltage magnitudes is highest. An iterative algorithm is proposed for finding this operating point. It considers both SNBs and SLLs and can be implemented using standard tools and solvers.

The performed case studies demonstrate the correct operation of the algorithm. However, current limitations exist that should be considered in the future: (i) The voltage magnitudes rely heavily on the proximity of the maximum loading point to the transfer limit surface. Future work could study alternatives to the repeated power flow calculations to find a point on the transfer limit surface rather than close to it. (ii) For some scenarios, the minimum voltage magnitude at the maximum loading point decreases over the iterations, see case studies 2 and 4. Alternatives to the linearized power flow equations could be explored that might lead to better calculations of the update vector. (iii) The performance generally depends on the initialization and the choice of hyperparameters, e.g., the step size. Future work could elaborate on how to choose the initial directions and settings to explore the search space adequately.

References

[1] E. Vrettos, M. Hohmann, and M. Zima, "A vision to enhance transmission security," *IEEE Power Energy Mag.*, vol. 19, no. 2, pp. 56–68, 2021.

[2] C. Vournas, "Technical Summary on the Athens and Southern Greece Blackout of July 12, 2004," Tech. Rep., Aug. 2004.

[3] "Voltage Stability Assessment: Concepts, Practices and Tools," IEEE Power & Energy Society, Tech. Rep. PES-TR9, Aug. 2002.

[4] R. J. Avalos, C. A. Cañizares, and M. F. Anjos, "A practical voltage-stability-constrained optimal power flow," in *2008 IEEE Power and Energy Society General Meeting - Conversion and Delivery of Electrical Energy in the 21st Century*, Pittsburgh, PA, 2008.

[5] C. Wang, B. Cui, Z. Wang, and C. Gu, "SDP-based optimal power flow with steady-state voltage stability constraints," *IEEE Trans. Smart Grid*, vol. 10, no. 4, pp. 4637–4647, 2019.

[6] X. Li, T. Jiang, L. Bai, X. Kou, F. Li, H. Chen, and G. Li, "Orbiting optimization model for tracking voltage security region boundary in bulk power grids," *CSEE Journal of Power and Energy Systems*, vol. 8, no. 2, pp. 476–487, 2022.

[7] Y. Kataoka and Y. Shinoda, "Voltage stability limit of electric power systems with generator reactive power constraints considered," *IEEE Trans. Power Syst.*, vol. 20, no. 2, pp. 951–962, 2005.

[8] P.-A. Löf, D. J. Hill, S. Arnborg, and G. Andersson, "On the analysis of long-term voltage stability," *International Journal of Electrical Power & Energy Systems*, vol. 15, no. 4, pp. 229–237, 1993.

[9] P. M. Anderson and A. A. Fouad, "The elementary mathematical model," in *Power System Control and Stability*, 2nd ed. Piscataway, NJ: Wiley-IEEE Press, 2003, ch. 2, pp. 13–52.

[10] B. Gao, G. Morison, and P. Kundur, "Voltage stability evaluation using modal analysis," *IEEE Trans. Power Syst.*, vol. 7, no. 4, pp. 1529–1542, 1992.

[11] I. Dobson, "Observations on the geometry of saddle node bifurcation and voltage collapse in electrical power systems," *IEEE Trans. Circuits Syst. I. Fundam. Theory Appl.*, vol. 39, no. 3, pp. 240–243, 1992.

[12] I. Dobson and L. Lu, "New methods for computing a closest saddle node bifurcation and worst case load power margin for voltage collapse," *IEEE Trans. Power Syst.*, vol. 8, no. 3, pp. 905–913, 1993.

[13] S. Greene, I. Dobson, and F. L. Alvarado, "Sensitivity of transfer capability margins with a fast formula," *IEEE Trans. Power Syst.*, vol. 17, no. 1, pp. 34–40, 2002.